Research in International Business and Finance 76 (2025) 102871

Contents lists available at ScienceDirect

Research in International Business and Finance

journal homepage: www.elsevier.com/locate/ribaf

Climate risk and renewable energy market volatility: Machine learning approach

Wei Jiang [a,1], Wanqing Tang [b,*,2], Jianfeng Li [c,3], Xiaokun Wei [d,*,4]

[a] School of Economics, Hangzhou Normal University, Hangzhou, China
[b] Business School of Hohai University, Nanjing, China
[c] College of Economics & Management, China Jiliang University, Hangzhou, China
[d] College of Economics and Management, Fujian Agriculture and Forestry University, Fuzhou, China

ARTICLE INFO

Keywords:
Climate risk
New-energy
Realized volatility
Deep-learning

ABSTRACT

Global climate change is a major environmental challenge, and the new-energy market is increasingly attracting investors' attention as a key area for investment, especially because of the impact of climate change on price volatility. In this study, we investigated the impact of climate change on China's new-energy market by introducing the following two indicators: China's climate policy uncertainty (CEU) indices and the climate uncertainty (CU) indices. We employed Diebold–Mariano and model confidence set tests to assess the out-of-sample prediction accuracy of our model. Empirical results showed that incorporating climate risk indices significantly improved the predictive accuracy of the three deep-learning models, with the CU index performing best in a variational modal decomposition (VMD)-long short-term memory (LSTM) model. In particular, in a VMD-LSTM model with the CU index indicator, the mean absolute error values for 1-, 3-, and 5-step ahead predictions were reduced by 8.1 %, 17.3 %, and 18.4 %, and the mean squared error values were reduced by 20.3 %, 40.0 %, and 32.4 %, respectively. Finally, the empirical findings remained robust, even when considering different estimation windows (historical training periods), forecast horizons (short-term, medium-term and long-term), and the impact of the COVID-19 pandemic.

1. Introduction

Global climate change is a major environmental challenge; therefore, investors seem to be increasingly attracted to the new-energy market for investments, especially due to the impact of climate change on price volatility. This study investigates the impact of climate change on China's new-energy market by introducing the following two indicators: China's climate policy uncertainty index and the climate uncertainty (CU) index. We employed Diebold–Mariano (DM) and model confidence set (MCS) tests to assess the out-of-sample prediction accuracy of each model. Empirical results showed that incorporating climate risk significantly improved the predictive

* Corresponding authors.
E-mail addresses: wjiang@hznu.edu.cn (W. Jiang), tarano_w@163.com (W. Tang), fengzhongfeifan@foxmail.com (J. Li), wxkjia1995@tongji.edu.cn (X. Wei).
[1] No. 2318 Yuhangtang Rd., Hangzhou 311121, China.
[2] No.8 Focheng West Rd., Nanjing 211100, China
[3] No.258, Xueyuan St., Hangzhou 310018
[4] No. 15, Shangxiadian Road, Fuzhou 350002

https://doi.org/10.1016/j.ribaf.2025.102871
Received 6 August 2024; Received in revised form 12 March 2025; Accepted 12 March 2025
Available online 15 March 2025

accuracy of the three deep-learning models (LSTM model, CNN-LSTM-attention model, and VMD-LSTM model), and the CU index performed best in a variational modal decomposition (VMD)-long short-term memory (LSTM) model. In particular, in a VMD-LSTM (VL) model with the CU index indicator, the mean absolute error (MAE) values were reduced by 8.1 %, 17.3 %, and 18.4 %, and the mean squared error (MSE) values were reduced by 20.3 %, 40.0 %, and 32.4 %, respectively. Finally, the empirical findings remained robust, even when we considered different estimation windows, forecast horizons, and the impact of the COVID-19 pandemic.

The volatility of new-energy market prices has received considerable attention because of the relative novelty of the market and the influence of various factors, such as the policy environment (Bonato et al., 2023; Karmakar et al., 2023). Volatility is often considered a measure of risk, and the level of volatility of prices in the new-energy market directly affects investor decisions and market stability (Gupta and Pierdzioch, 2022). Therefore, accurately predicting the volatility of new-energy market prices is crucial for financing.

Climate change has become a major global concern that not only directly affects the environment and society but also profoundly impacts the stability and volatility of financial markets (Jin et al., 2020; Tian et al., 2022; Wang and Li, 2023; Xia et al., 2022; Xu and Zhang, 2023). Climate risk has been identified as a key factor that affects portfolios and market risk (Gu et al., 2024; Liang et al., 2022; Sadorsky, 2022). For quantification purposes, the Task Force on Climate-related Financial Disclosure classifies the risks posed by climate change as physical or transition. Physical risk arises from extreme weather and natural disasters that can lead to a loss of financial trading assets and collateral damage, and covers both sudden events (e.g., heat waves, floods, and hurricanes) and long-term trends (e.g., sea level rise, changes in precipitation patterns, and temperature increases). Transition risk involves shifts in laws, policies, technologies, and consumer preferences as societies move toward sustainable development. These two types of risk intersect, affecting the stability of financial markets (Bonato et al., 2023; Guo et al., 2023; Huang et al., 2023).

The connection between climate change and the new-energy market is particularly strong, as the new-energy market is not only a major driving force in combating climate change but also a field directly affected by climate change. Extreme weather events, rise in global greenhouse gas emissions, and climate policies implemented by governments profoundly alter the structure of energy demand and supply patterns. In this context, traditional energy sources, such as oil and natural gas, face greater supply uncertainties and cost pressures, whereas new-energy sources, owing to their environmental friendliness and renewability, have become a focus of policy support and technological innovation, causing the rapid expansion of the new-energy market. Studies have shown that climate risk is a factor that affects companies' share prices, while major climate policy changes trigger volatility in energy companies' prices (Bartram et al., 2022; Berkman et al., 2024; Li et al., 2019). Furthermore, policy and physical risks triggered by climate change introduce volatility into the new-energy market, affecting investors' decisions. Hence, an in-depth study of the impact of climate change on the volatility of new-energy market prices can provide both a forward-looking reference for investors and a basis for policymakers to address climate risk.

Drawing from the study by Wang and Li (2023), we selected CU and CEU indices proposed by Lee and Cho (2023) to measure physical and transition risks, respectively, for comprehensively assessing the effects of climate risk on China's new-energy stock market.

The new-energy market addresses climate change and deals with fuel scarcity issues, and it is driven by policy support and technological innovation as a major investment direction in financial markets (Fan et al., 2024; Hertwich et al., 2015). The new-energy market is similarly affected by the new risk factor: CU index. The complexity and diversity of climate change and changes in climate policy lead to an uncertainty that gives rise to instability in related areas such as energy production and consumption. Furthermore, extreme weather events triggered by climate change can directly affect the production and distribution of traditional energy sources, leading to supply instability, reduced production capacity, and increased transportation costs for traditional energy companies. New-energy sources, which are relatively independent of climatic factors and have lower risk profiles than traditional sources, have increased the competition in the energy market, thereby affecting the balance between supply and demand. This imbalance has directly impacted the financial positions and market performances of companies and triggered price volatility, where market participants dynamically recalibrate asset valuations in alignment with evolving climate risk exposures. Furthermore, such imbalance may lead to volatility in energy prices, thereby affecting profitability and investor sentiment in the new-energy market (Guo et al., 2022). For example, investors may adjust their portfolios to focus more on environmental and sustainability factors in the face of climate risk (Lv and Li, 2023). New-energy technologies, as a key path to achieving the goals of "peak carbon" and "carbon neutrality," have attracted a large amount of capital into the new-energy market, thus improving the performance of new-energy operators. All of these factors can lead to volatility in the share prices of new-energy companies.

Studies have shown that climate policies and major climate events are associated with volatility in financial markets. Several studies have focused on the impact of climate on nonferrous metal markets, such as those of gold (Gupta and Pierdzioch, 2022; Karmakar et al., 2023; Salisu et al., 2023), and other energy markets (Guo et al., 2023; Isah et al., 2023; Liang et al., 2022; Rao et al., 2023). Their findings emphasized the importance of considering climate change as a key factor in forecasting models to predict market volatility accurately, help companies and investors assess risk precisely, and formulate business strategies accordingly, thereby reducing losses and increasing investment returns. Therefore, analyzing the role of climate risk in predicting the realized volatility (RV) of China's new-energy market is vital.

For forecasting analysis, most studies adopt econometric models, such as the GARCH family and HAR, in their research

methodology. However, these models must satisfy certain statistical assumptions before modeling and demonstrate limitations when they face time-series data with highly complex characteristics such as nonlinearity and nonsmoothness. Deep-learning models overcome this problem, and academics have widely recognized the former's high performance in handling high-frequency RV with long-memory characteristics (Gamboa, 2017). LSTM recurrent neural network models effectively transmit and express information over extended periods without forgetting earlier information. Thus, they excel at characterizing time-series data with long-memory properties. Previous studies have also confirmed their superiority in volatility prediction (Kristjanpoller, 2024; Liu, 2019).

The attention mechanism (a computational technique that enables models to dynamically prioritize and focus on the most relevant parts of input data by assigning context-dependent weights to different elements) is a widely used concept and an effective tool in deep-learning. Accurate prediction can be achieved by mining coarse-grained features containing longer memory information with LSTM after initial extraction by a convolutional neural network (CNN) based on the attention mechanism (Li et al., 2019). The VMD method proposed by Dragomiretskiy and Zosso (2014) fully considers the narrow-band nature of components, as its filtering band is concentrated and decomposed components have high signal-to-noise ratios. Thus, the feature information input to the prediction model is quite adequate, and combining the VMD method with the LSTM model can provide increasingly accurate predictions (He et al., 2019; Jiang et al., 2023; Liu et al., 2020).

Therefore, for this study, we selected the following three representative new-energy indices in China: CSI New-Energy, CNI New-Energy, and CN New-Energy indices. Furthermore, we applied the following three deep-learning models: LSTM, CNN-LSTM-attention (CLA), and VL. In addition, we incorporated climatic factors into the volatility prediction framework to explore their volatility prediction ability in the Chinese new-energy market. Furthermore, we explored the role of climatic factors in the volatility forecasting framework of the Chinese new-energy market.

Compared with previous research, this study makes several contributions. First, for the volatility prediction of the Chinese new-energy market, this study adopted a deep-learning model that can handle nonlinear and nonstationary time-series data. This model performs better than the traditional GARCH and HAR-type models for predicting volatility. Second, we selected 5-minute high-frequency data from the China New-Energy Index for volatility prediction. Such data can better reflect intraday volatility information than low frequency data such as daily data (Andersen et al., 2005). In addition, to improve its prediction accuracy, this study introduced the VL model that combines the data decomposition algorithm VMD with the LSTM model to address the microstructural noise problem in the RV that is computed based on high-frequency data. The results showed that the VL model performed best in terms of predicting the RV of the China New-Energy Index in all analyses. Third, this study incorporated climatic factors and evaluated the forecasting effectiveness of the CEU and CU indices using different new-energy indices. Both the CEU and CU indices effectively improved the forecasting accuracy of RV in the Chinese new-energy market. In particular, the CU index was more effective in improving the forecasting of CSI New-Energy and CNI New-Energy indices, whereas the CEU index was more effective in improving the forecasting of the CN New-Energy Index. Hence, this study provides a new perspective for accurately predicting the RV of the Chinese new-energy market and acknowledges the importance of climate risk assessment in portfolio management in the capital market, thus providing valuable information for the fields of climate risk and the energy market.

Compared to existing studies, this study is innovative in the following ways:

(1) **Incorporation of climate risk:** By quantifying and integrating climate risk into the volatility forecasting of new-energy markets prices, this study enriched the climate-integrated analytical framework, establishing novel methodologies for incorporating climate risk factors into volatility forecasting models, providing the first systematic exploration in the field of new-energy.
(2) **Diversity of models:** This study employed three deep-learning models, and through comparison, it investigated the effectiveness of these models in predicting the volatility of new-energy markets under climate risk.

The remainder of this article is organized as follows: Section 2 introduces various methods used in this study. Section 3 presents the data selected for this study and provides a preliminary analysis of the data. Section 4 presents the empirical research results that verified the impact of climate risk on the volatility prediction of the Chinese new-energy market prices through the loss indicators: DM and MCS tests. Finally, Section 5 concludes the study.

2. Modeling approach

2.1. Introduction of RV

We selected the 5-minute intraday high-frequency data from Chinese crude oil futures to construct RV. For the first t day, $RV(t)$, the sum of the squared intraday high-frequency returns is represented as follows:

$$RV(t) = \sum_{j=1}^{M} r_{t,j}^2 \quad (1)$$

where M is the sampling frequency; $r_{t,j} = \ln P_{t,j} - lnP_{t,j-1}$ is the sampling frequency of the t day of the j intraday return; and $P_{t,j}$ is the first t day j closing price.

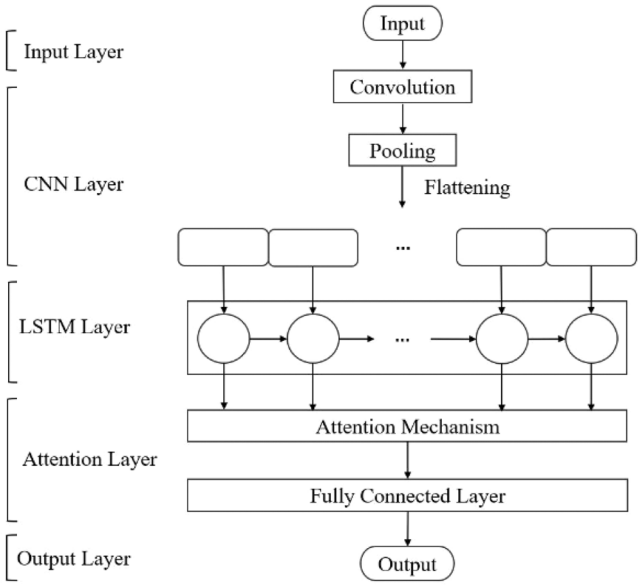

Fig. 1. CNN-LSTM-Attention mechanism.

2.2. Introduction of LSTM model

As its neural network is good at capturing long-term dependencies, LSTM is a suitable deep-learning method for time-series prediction. In the LSTM memorization method for long-term memory, the forgetting gate is close to one if important information is absent, and the updating gate is close to one if important information is present. The basic steps of LSTM are as follows:

First, the forgetting gate h_t filters and retains historical information that indicates long-term trends and discards noncritical information:

$$f_t = \sigma\left(W_f \cdot [h_{t-1}, X_t] + b_f\right) \tag{2}$$

where W indicates the corresponding weight matrices, b is the corresponding bias term, and $\sigma(\cdot)$ represents the sigmoid function.

Second, the update gate i_t at time t from the input X_t extracts new information, and according to the hyperbolic tangent activation function, $\tanh(\cdot)$ creates a candidate value $\widetilde{C}_t$ to update the state:

$i_t = \sigma(W_i \cdot [h_{t-1}, X_t] + b_i)(3)\widetilde{C}_t = \tanh(W_c \cdot [h_{t-1}, X_t] + b_c)$(4)

Then, in the update gate, the old cell state is updated by removing some information from the old cell and adding filtered candidate values C_{t-1} that are updated to the new cell state C_t:

$$C_t = f_t * C_{t-1} + i_t * \widetilde{C}_t \tag{5}$$

where $*$ denotes the dot product between matrices.

Subsequently, the output gate o_t filters the updated C_t, and filtering is performed as follows:

$$o_t = \sigma(W_o \cdot [h_{t-1}, X_t] + b_o) \tag{6}$$

Finally, the final output is calculated based on the new state and output gate state:

$$h_t = o_t \cdot \tanh(C_t) \tag{7}$$

2.3. Introduction of CLA model

2.3.1. CNN models

CNN models take advantage of convolutional operations to provide high-level and abstract representations of the original data and extract local features of the data effectively. Its basic structure consists of an input layer (input layer), a convolution layer (convolution layer), a pooling layer (pooling layer), and a fully connected layer (full-connection layer). The core structure of the convolution layer is a filter that enhances the extracted signal features and reduces noise interference. The formula for the convolution process is as follows:

$$C = f(X \otimes W + b) \tag{8}$$

where X is the input data, W is the weight vector of the convolution kernel, b is the bias, $\otimes$ is the convolution computation, and $f(\cdot)$ is the activation function (ReLu function in this study).

The pooling layer further aggregates the feature combinations from multiple windows to reduce the number of nodes in the fully connected layer while effectively retaining the main features of the extracted data, thereby simplifying the network parameters and preventing overfitting.

In this study, a CNN was used to extract the original data features and remove the noise and unstable components from them, and the processed relatively stable information was passed into the LSTM layer for long-sequence prediction.

2.3.2. Attention mechanism

The attention mechanism is a widely used concept and an effective tool in deep-learning that originates from the study of vision. It was proposed with reference to the operation of the human brain. The attention mechanism can help identify important information during the deep-learning process. The method of probability assignment, which can replace the original random weight assignment with the method of assigning probabilities, can be based on the input of the k, feature vector h_i, and the environment vector obtained by c_i, and the model can obtain the environment vector based on the inputs as follows:

$$c_i = \sum_{i=1}^{k} \alpha_i h_i \tag{9}$$

where $\alpha_i$is the attention weight, denoted as the follows:

$$\alpha_i = Softmax(S_i) = \frac{e^{S_i}}{\sum j e^{S_i}} \tag{10}$$

where S_i denotes c_i and h_i the degree of correlation.

In this study, the output matrix of each step of the LSTM layer was calculated using the Softmax function to obtain the weight matrix of the output of each step, which was then multiplied by the matrix to complete the introduction of attention.

2.3.3. CLA model construction

The CLA model comprises the following three parts: CNN, LSTM, and attention layers. Fig. 1 depicts the specific mechanism.

2.4. Introduction of VL model

Previous studies have shown that applying data decomposition techniques to the original $RV(t)$ sequence decomposition can reduce the influence of noise on RV prediction. Considering the better prediction effect of the VL model based on the data decomposition technique and deep-learning LSTM, we selected the VL model to predict the RV of the new-energy index for this study, which is briefly described as follows:

2.4.1. VMD

The VMD method proposed by Dragomiretskiy and Zosso (2014) is a nonrecursive variational mode signal decomposition method with an overall framework as a variational problem. This method has a unique advantage in the form of its capability to specify the number of modes that one wants to obtain by effectively avoiding mode aliasing (The phenomenon of non-physical overlap between different intrinsic mode functions during the decomposition process is manifested when a single mode contains multiple characteristic frequency components or when multiple modes share similar frequency bands) and endpoint effects (The boundary distortion phenomenon occurring at the beginning and end of a time series during signal decomposition). The essence of VMD is the construction and solving of a variational problem with the constrained variational model as follows:

$$\begin{cases} \min\limits_{\{u_k\},\{\omega_k\}} \left\{ \sum\limits_k \left\| \partial_t \left[\left(\delta(t) + \dfrac{j}{\pi t} \right) * u_k(t) \right] e^{-j\omega_k t} \right\|_2^2 \right\} \\ s.t. \sum\limits_k u_k = f \end{cases} \tag{11}$$

where $\{u_k\} = \{u_1, \cdots, u_k\}$ represents the modal components obtained after the decomposition of the original sequence, and $\{\omega_k\} = \{\omega_1, \cdots, \omega_k\}$ represents the center frequency of each modal component. To find the optimal solution for the previous constrained variational model, it must be converted into an unconstrained problem and solved. We introduced the Lagrange multiplier operator in Eq. (11) and $\lambda(t)$ with a quadratic penalty factor ∂ for conversion into an unconstrained variational model.

$$L(\{u_k\},\{\omega_k\},\lambda) := \alpha\sum_k \left\| \partial_t \left[\left(\delta(t) + \frac{j}{\pi t}\right) * u_k(t) \right] e^{-j\omega_k t} \right\|_2^2 + \left\| f(t) - \sum_k u_k(t) \right\|_2^2 + \left\langle \lambda(t), f(t) - \sum_k u_k(t) \right\rangle \tag{12}$$

We obtained the optimal solution of Eq. (12) by iteratively updating the modal components and their corresponding center frequencies using the alternating-direction method of multipliers. The optimal solutions for the modal components and center frequencies are as follows:

$$\begin{cases} \hat{u}_k^{n+1}(\omega) := \dfrac{\hat{f}(\omega) - \sum_{i\neq k}\hat{u}_i(\omega) + \dfrac{\hat{\lambda}(\omega)}{2}}{1 + 2\alpha(\omega - \omega_k)^2} \\ \omega_k^{n+1} := \dfrac{\int_0^{+\infty} \omega |\hat{u}_k(\omega)|^2 d\omega}{\int_0^{+\infty} |\hat{u}_k(\omega)|^2 d\omega} \end{cases} \tag{13}$$

where ω represents frequency, $\hat{u}_k^{n+1}$, and $\hat{f}(\omega)$,$\hat{u}_k(\omega)$and $\tilde{\lambda}(\omega)$ correspond to the Fourier transforms of u_k^{n+1},$f(\omega)$,$u_k(\omega)$and $\lambda(\omega)$, respectively.

2.4.2. VL model construction

As mentioned previously, due to the significant noise issues associated with high-frequency RV, directly use historical RV data for forecasting would reduce the accuracy of the forecast. VMD can decompose an original RV series into intrinsic mode function (IMF) components, decompose these components, and then perform prediction modeling on the decomposed components separately to reduce the error caused by noise, thereby improving prediction accuracy. However, some studies ignored the residual components after VMD (Abdoos, 2016; Lahmiri, 2017), which prevented complex information contained in the residual components from serving as input into prediction models. Therefore, this study incorporated decomposed residuals into an LSTM model for prediction to ensure that the effective information in high-frequency data is fully utilized. This process included three steps.

In Step 1, we used the VMD algorithm to decompose an original $RV(t)$ sequence into several IMF components, and then we subtracted the original sequence from the individual IMF components to obtain the remaining residual term of the VMD.

In Step 2, we divided the dataset into training, validation, and prediction sets. Subsequently, we used the data from the training set as input into the corresponding LSTM prediction model for training and the data from the validation set to test the generalization performance of the model. Finally, data from the prediction set were used to obtain the following prediction results: $\widehat{IMF_t}(t)$ and $\widehat{R(t)}$.

In Step 3, we obtained a final prediction sequence by reconstructing all the prediction results using Eq. (14) as follows:

$$\widehat{RV(t)} = \sum_{i=1}^{n} \widehat{IMF_i}(t) + \widehat{R(t)}, t = X+Y+1, X+Y+2, \ldots, X+Y+H \tag{14}$$

where X is the length of the training set, Y is the length of the validation set, H is the length of the prediction set, and $\widehat{R(t)}$ is the final prediction sequence.

Owing to VMD's ability to decompose signals into narrow-band IMFs, this hybrid model significantly outperformed other models in predicting lagging and peak values. By focusing on the narrow-band properties of the components, the VMD achieved a more concentrated filtering frequency band, which then enhanced the signal-to-noise ratio of the IMFs. Consequently, the feature information passed as input data onto the LSTM model was richer than that provided by other decomposition methods, allowing the LSTM model to predict more accurately, capitalizing on the high-quality features extracted through the effective decomposition process of VMD. Thus, the VL model leveraged the strengths of both the precise signal analysis of VMD and the capability of LSTM to capture temporal dependencies, thereby offering a powerful tool for forecasting in various domains.

2.5. Out-of-sample assessment methodology

This study aimed to assess whether including CEU and CU indices improves the accuracy of prediction models. Therefore, in this study, the three prediction methods mentioned above are first applied without incorporating climate risk indices. To ensure the robustness of the results, we followed the methodology of Herrera et al. (2022) to perform one step, three-step, and five-step-ahead forecasts, representing short-, medium-, and long-term periods, respectively.

We used MAE and MSE to measure the prediction error as follows:

Table 1
Descriptive statistics for climate risk indicators.

Variable	Mean	Std. Dev	Skewness	Kurtosis
CEU	0.057	0.122	4.871	28.631
CU	0.151	0.196	2.049	4.093

Table 2
Descriptive statistics of the realized volatility (RV) of the new-energy indices.

Index	CSI New-Energy	CNI New-Energy	CN New-Energy
Count	1821	1821	1522
Mean	0.015	0.014	0.015
Std. Dev	0.014	0.014	0.014
Skewness	1.993	2.015	1.935
Kurtosis	5.236	5.518	5.565
JB	$3.29 \times 10^{3***}$	$3.54 \times 10^{3***}$	$2.91 \times 10^{3***}$
Q(10)	$6.29 \times 10^{2***}$	$5.04E \times 10^{2***}$	$4.48 \times 10^{2***}$

Note: JB denotes the Jarque–Bera statistic; Q (10) denotes the Ljung–Box statistic of the lagged 10th order; and *, **, and *** denote significance levels at the 10 %, 5 %, and 1 %, respectively.

$$MAE = H^{-1}\sum_{t=1}^{H}|y-\widehat{y}| \tag{15}$$

$$MSE = H^{-1}\sum_{t=1}^{H}(y-\widehat{y})^2 \tag{16}$$

where H is the total length of the predicted sample, y_t is the true value, and $\widehat{y}_t$ is the predicted value. The lower the values of MAE and MSE, the higher the accuracy of the prediction model.

2.5.1. Diebold–Mariano (DM) test

We used the DM test proposed by Diebold and Mariano (2002) to determine whether the difference in the predictions between the two models was statistically significant. Using this test, we compared the results of two predictive models at a time and tested the original hypothesis at the same level of accuracy. If the results indicated a need to reject the original hypothesis, the test confirmed that a statistically significant difference existed between the models.

Assuming that the prediction errors of the two models are $\mu_{1,t}$ and $\mu_{2,t}$, $\varphi(\mu_{1,t},t)$ and$\varphi(\mu_{2,t},t)$ represent their loss functions, respectively, as follows:

$$d_t = \varphi(\mu_{1,t}) - \varphi(\mu_{2,t}) \tag{17}$$

To ascertain which of the two models had better predictive power, the original hypothesis was set to "*no difference in model predictive ability*" as follows:

$$H_0 : E(d_t) = 0 \tag{18}$$

The sequence of loss variances $\{d_t\}$can be used to infer the asymptotic distribution of the mean of the sample loss variance, which, according to the central limit theorem, $\{d_t\}$ can be assigned as follows:

$$\sqrt{T}(\overline{d}-u) \xrightarrow{d} N(0, 2\pi f_d(0)) \tag{19}$$

where $\overline{d} = \frac{1}{H}\sum_{t=1}^{H} d_t$ is the average value of the sample loss difference; $f_d(0) = \frac{1}{2\pi}\sum_{t=-\infty}^{+\infty} r_d(\tau)$is the spectral line density when the loss difference frequency is zero; $u = E(d_t)$ is the overall mean of the loss difference; and $r_d(\tau) = E[(d_t - u)(d_{t-\tau} - u)]$ is the overall mean of the d_t first-order autocorrelation of the τ order autocorrelation of the samples. The test statistic is as follows:

$$DM = \frac{\overline{d}}{\sqrt{\frac{2\pi\widehat{f}_d(0)}{H}}} \tag{20}$$

where $\widehat{f}_d(0)$ is $f_d(0)$ a consistent estimate. Hence, under the original assumption that the two models have the same predictive power, the DM statistic followed a standard normal distribution.

2.5.2. MCS test

Loss-function values do not provide statistical information about the existence of a significant difference in the predictive per-

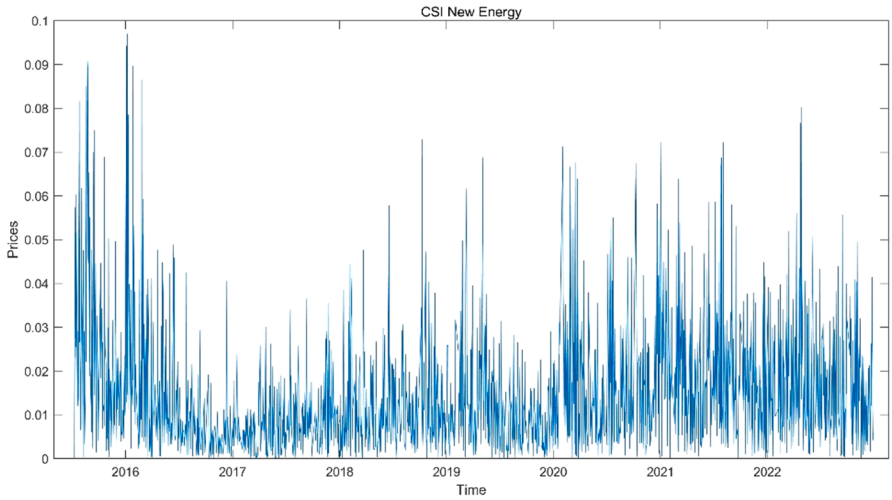

(a) CSI New-Energy Index

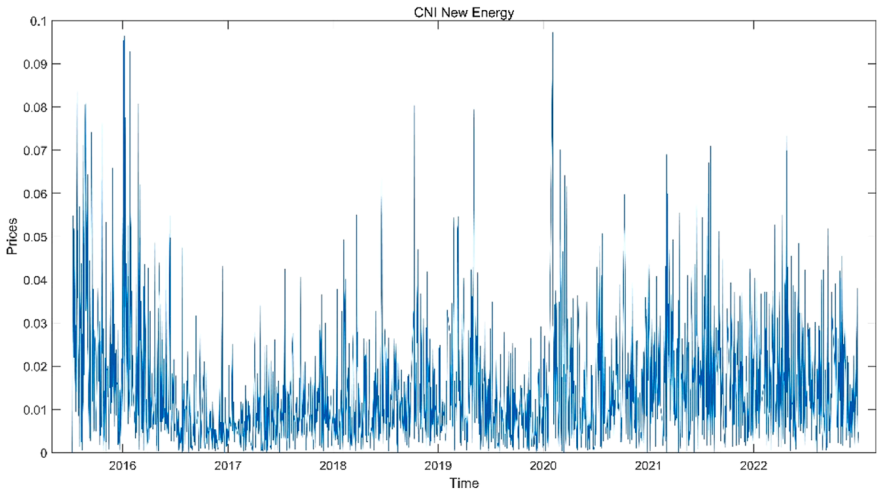

(b) CNI New-Energy Index

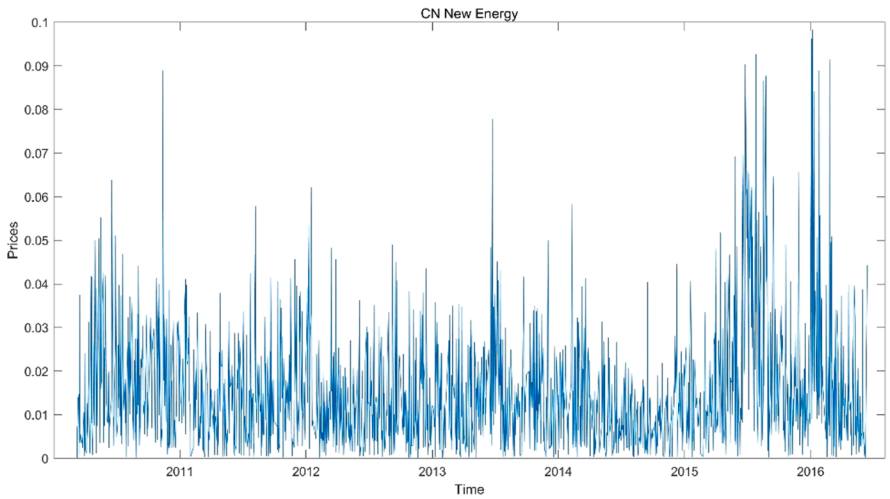

(c) CN New-Energy

(caption on next page)

Fig. 2. Chinese New-Energy Index RV series.

Table 3
K values of IMFs center frequency.

K	Center frequency										
Plan A: CSI New-Energy											
1	0.000										
2	0.001	0.293									
3	0.001	0.363	0.460								
4	0.001	0.195	0.334	0.428							
5	0.001	0.204	0.291	0.373	0.452						
6	0.000	0.069	0.203	0.297	0.380	0.457					
7	0.000	0.064	0.143	0.228	0.313	0.385	0.460				
8	0.000	0.041	0.116	0.199	0.269	0.335	0.395	0.464			
9	0.000	0.088	0.159	0.231	0.298	0.355	0.404	0.455	**0.489**		
10	0.000	0.067	0.136	0.204	0.267	0.320	0.367	0.410	0.456	0.489	
11	0.000	0.063	0.117	0.166	0.223	0.282	0.329	0.375	0.416	0.458	0.489
Plan B: CNI New-Energy											
1	0.000										
2	0.001	0.299									
3	0.001	0.373	0.463								
4	0.001	0.295	0.404	0.479							
5	0.001	0.226	0.304	0.380	0.453						
6	0.001	0.192	0.246	0.318	0.386	0.458					
7	0.000	0.060	0.139	0.228	0.306	0.383	0.457				
8	0.000	0.039	0.118	0.200	0.267	0.330	0.391	0.461			
9	0.000	0.091	0.161	0.238	0.302	0.361	0.407	0.455	**0.488**		
10	0.000	0.064	0.129	0.202	0.263	0.314	0.366	0.410	0.455	0.488	
11	0.000	0.063	0.119	0.173	0.230	0.289	0.339	0.381	0.420	0.458	0.488
Plan C: CN New-Energy											
1	0.000										
2	0.001	0.440									
3	0.001	0.368	0.465								
4	0.001	0.072	0.288	0.400							
5	0.001	0.239	0.357	0.427	0.482						
6	0.001	0.067	0.191	0.303	0.385	0.453					
7	0.000	0.060	0.146	0.241	0.317	0.388	0.455				
8	0.000	0.068	0.150	0.234	0.299	0.367	0.429	0.481			
9	0.000	0.069	0.149	0.233	0.294	0.355	0.398	0.440	0.484		
10	0.000	0.066	0.138	0.202	0.258	0.311	0.361	0.397	0.433	**0.473**	
11	0.000	0.058	0.108	0.161	0.223	0.271	0.319	0.364	0.398	0.434	0.473

formance of models; hence, the results obtained using these values only as judgment criteria are not robust. To obtain more robust test results, we adopted the MCS test as an out-of-sample predictive power test for each model to enable a direct comparison of the different models (Hansen et al., 2011). In addition, we selected the commonly used range statistic T_R and semiquadratic statistic T_{SQ} as test criteria in this study as follows:

$$T_R = \max_{i,j \in M} \frac{|\overline{d_{ij}}|}{\sqrt{var(\overline{d_{ij}})}} \tag{21}$$

$$T_{SQ} = \max_{i,j \in M} \frac{(\overline{d_{ij}})^2}{\sqrt{var(\overline{d_{ij}})}} \tag{22}$$

$$\overline{d_{ij}} = H^{-1} \sum_{t=1}^{H} d_{ij,t} \tag{23}$$

where $\overline{d_{ij}}$ represents the average value of the relative loss function between the predicted values of model i and j.

We initially employed a standard LSTM model configuration to establish a baseline for the analysis. However, architecture and hyperparameter selection played decisive roles in determining the model's effectiveness, which might have limited the study.

To address this issue and improve the robustness and accuracy of our model, we plan to incorporate more systematic approaches (like dynamic hyperparameter tuning via Bayesian optimization) to optimize deep-learning architecture in future research.

In particular, we will explore techniques such as grid search, random search, and more advanced methods such as Bayesian optimization to systematically optimize key hyperparameters, such as the number of hidden units, learning rate, batch size, and

Table 4
Descriptive statistics of RV series decomposition results.

	Mean	Std. Dev	Skewness	Kurtosis	Q (10)
Panel A: CSI New-Energy					
IMF1	1.25×10^{-8}	3.23×10^{-3}	0.001	1.588	$1.45 \times 10^{4***}$
IMF2	1.44×10^{-8}	4.08×10^{-3}	0.003	0.902	$6.84 \times 10^{3***}$
IMF3	1.82×10^{-8}	4.11×10^{-3}	0.008	1.305	$7.09 \times 10^{3***}$
IMF4	2.36×10^{-8}	4.12×10^{-3}	0.043	1.180	$7.12 \times 10^{3***}$
IMF5	3.37×10^{-8}	3.88×10^{-3}	0.013	1.341	$6.93 \times 10^{3***}$
IMF6	5.63×10^{-8}	3.71×10^{-3}	0.010	3.658	$6.28 \times 10^{3***}$
IMF7	1.19×10^{-7}	3.62×10^{-3}	0.023	0.979	$6.71 \times 10^{3***}$
IMF8	3.85×10^{-7}	3.92×10^{-3}	0.140	1.392	$6.02 \times 10^{3***}$
Res	1.45×10^{-2}	6.70×10^{-3}	1.130	1.987	$1.63 \times 10^{4***}$
Panel B: CNI New-Energy					
IMF1	1.19×10^{-8}	3.31×10^{-3}	0.002	1.146	$1.40 \times 10^{4***}$
IMF2	1.37×10^{-8}	3.95×10^{-3}	0.003	1.249	$6.94 \times 10^{3***}$
IMF3	1.71×10^{-8}	4.17×10^{-3}	0.007	0.770	$7.07 \times 10^{3***}$
IMF4	2.16×10^{-8}	4.12×10^{-3}	0.037	2.058	$6.93 \times 10^{3***}$
IMF5	3.09×10^{-8}	3.99×10^{-3}	0.024	1.486	$6.98 \times 10^{3***}$
IMF6	5.02×10^{-8}	3.84×10^{-3}	0.009	2.761	$6.52 \times 10^{3***}$
IMF7	1.10×10^{-7}	3.58×10^{-3}	0.028	0.628	$6.61 \times 10^{3***}$
IMF8	3.41×10^{-7}	3.91×10^{-3}	0.112	1.067	$6.23 \times 10^{3***}$
Res	1.44×10^{-2}	6.27×10^{-3}	1.179	2.171	$1.61 \times 10^{4***}$
Panel C: CN New-Energy					
IMF1	1.46×10^{-8}	3.50×10^{-3}	0.002	1.043	$5.92 \times 10^{3***}$
IMF2	1.74×10^{-8}	3.50×10^{-3}	0.001	1.411	$6.81 \times 10^{3***}$
IMF3	2.06×10^{-8}	3.42×10^{-3}	0.006	1.815	$6.76 \times 10^{3***}$
IMF4	2.50×10^{-8}	3.60×10^{-3}	0.021	1.316	$6.06 \times 10^{3***}$
IMF5	3.36×10^{-8}	3.63×10^{-3}	0.022	0.347	$5.89 \times 10^{3***}$
IMF6	4.89×10^{-8}	3.67×10^{-3}	0.009	0.792	$5.89 \times 10^{3***}$
IMF7	7.98×10^{-8}	3.52×10^{-3}	0.007	0.204	$5.97 \times 10^{3***}$
IMF8	1.70×10^{-7}	3.78×10^{-3}	0.019	0.968	$5.34 \times 10^{3***}$
IMF9	7.38×10^{-7}	4.11×10^{-3}	0.202	4.162	$5.88 \times 10^{3***}$
Res	1.53×10^{-2}	6.40×10^{-3}	1.972	4.936	$1.37 \times 10^{4***}$

Note: Kurtosis is excess kurtosis; Q (10) denotes the lagged 10th-order Ljung–Box statistic; *, **, and *** denote significance at the 10 %, 5 %, and 1 % levels, respectively.

dropout rate. We aim to apply such optimization strategies not only to enhance the predictive power of the LSTM model but also to improve its generalizability across different datasets and contexts, ensuring its robustness in real-world applications.

3. Data and preliminary analyses

In this study, we explored the impact of CEU and CU indices on the predicted performance of a new-energy index. We obtained CEU and CU indices' data from https://sites.google.com/view/twitter-chn-epu/home. To eliminate differences in magnitude, we scaled the raw CEU and CU indices using normalization, and Table 1 presents their descriptive statistics. Previous studies have shown that 5-minute high-frequency data can balance the requirement of high-frequency samples and reduce micronoise (Andersen and Bollerslev, 1998). Therefore, we selected 5 minutes as the sample frequency in this study. According to the availability of data, we selected the sampling periods for CSI New-Energy and CNI New-Energy from July 10, 2015, to December 30, 2022. As the sample period for CN New-Energy, we selected the duration from March 9, 2010, to June 13, 2016, and obtained the index data from the RESSET database. Then, using Eq. (1), were calculated realized volatilities of all three indices.

Table 2 presents the descriptive statistics of the RV series for the three new-energy indices. The realized volatilities of the new-energy indices exhibited significant leptokurtic and skewed characteristics. The Jarque–Bera (JB) statistic indicated that the realized volatilities had a significant non-normal distribution, while the Ljung–Box statistic showed that the original hypothesis of no autocorrelation within the lagged 10th order was rejected at the 1 % significance level, indicating that the realized volatilities for all of China's new-energy indices had significant long-memory characteristics. The realized volatilities exhibited significant long-term memory characteristics. Fig. 2 shows the time-series plots of the realized volatilities of the three new-energy indices.

To forecast the RV of the new-energy index using the VL model, we decomposed the original series into several components and a residual term using the VMD algorithm, followed by inputting the resulting subsequence into the LSTM model for forecasting. Given the special characteristics of the VMD algorithm, we had to determine the number of modal decomposition layers before they could be used for data decomposition K. In this study, we used the center frequency method proposed by Huang et al. (2019) to determine the number of decomposition layers (K).

Table 3 lists the IMFs of the three new-energy indices for different values, and Table 4 shows the center frequencies of the three new-energy indices. Because similar frequencies are stable after 9, 9, and 10, according to the principle of the center frequency method, we set the modal decomposition layers of the new-energy indices to 8, 8, and 9, respectively.

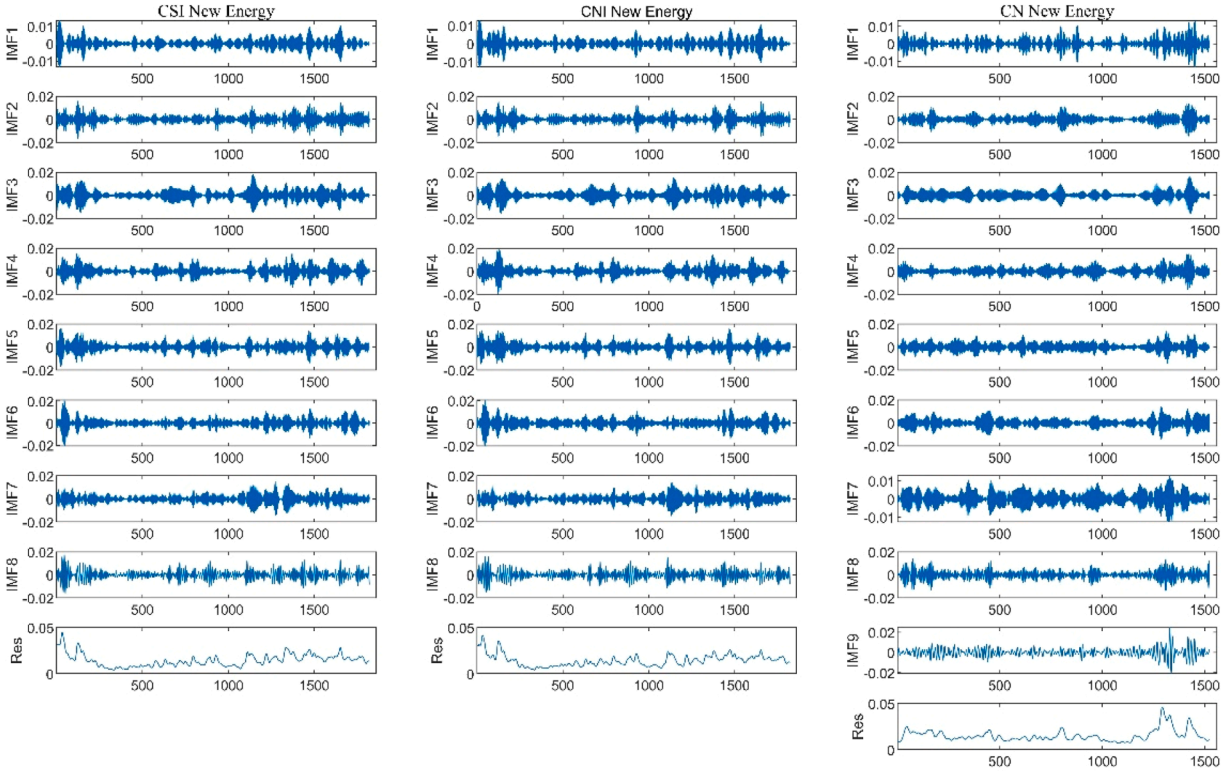

Fig. 3. VMD results.

Table 5
Predictive evaluation results under different loss functions.

Models	CSI New-Energy		CNI New-Energy		CN New-Energy	
	MAE	MSE	MAE	MSE	MAE	MSE
Panel A: H = 1						
LSTM	1.08×10^{-2}	2.33×10^{-4}	1.03×10^{-2}	2.14×10^{-4}	1.25×10^{-2}	3.73×10^{-4}
LSTM-CEU	1.07×10^{-2}	2.27×10^{-4}	1.02×10^{-2}	2.06×10^{-4}	1.24×10^{-2}	3.72×10^{-4}
LSTM-CU	1.06×10^{-2}	2.15×10^{-4}	1.01×10^{-2}	1.96×10^{-4}	1.23×10^{-2}	3.80×10^{-4}
CLA	1.17×10^{-2}	2.41×10^{-4}	1.12×10^{-2}	2.25×10^{-4}	1.51×10^{-2}	5.18×10^{-4}
CLA-CEU	1.09×10^{-2}	2.29×10^{-4}	1.03×10^{-2}	2.13×10^{-4}	1.23×10^{-2}	3.85×10^{-4}
CLA-CU	1.07×10^{-2}	2.24×10^{-4}	1.03×10^{-2}	1.99×10^{-4}	1.34×10^{-2}	4.27×10^{-4}
VL	8.36×10^{-3}	1.21×10^{-4}	8.86×10^{-3}	1.44×10^{-4}	1.03×10^{-2}	2.13×10^{-4}
VL-CEU	7.72×10^{-3}	9.73×10^{-5}	7.38×10^{-3}	8.90×10^{-5}	8.38×10^{-3}	1.43×10^{-4}
VL-CU	7.68×10^{-3}	9.64×10^{-5}	7.33×10^{-3}	8.79×10^{-5}	8.40×10^{-3}	1.44×10^{-4}
Panel B: H = 3						
LSTM	1.13×10^{-2}	2.28×10^{-4}	1.08×10^{-2}	2.09×10^{-4}	1.23×10^{-2}	3.96×10^{-4}
LSTM-CEU	1.12×10^{-2}	2.13×10^{-4}	1.07×10^{-2}	1.98×10^{-4}	1.22×10^{-2}	3.74×10^{-4}
LSTM-CU	1.11×10^{-2}	2.10×10^{-4}	1.04×10^{-2}	1.96×10^{-4}	1.21×10^{-2}	3.87×10^{-4}
CLA	1.44×10^{-2}	3.24×10^{-4}	1.11×10^{-2}	2.06×10^{-4}	1.68×10^{-2}	5.52×10^{-4}
CLA-CEU	1.12×10^{-2}	2.14×10^{-4}	1.08×10^{-2}	1.95×10^{-4}	1.20×10^{-2}	3.71×10^{-4}
CLA-CU	1.11×10^{-2}	2.12×10^{-4}	1.07×10^{-2}	1.93×10^{-4}	1.23×10^{-2}	3.70×10^{-4}
VL	4.27×10^{-3}	3.04×10^{-5}	6.17×10^{-3}	6.11×10^{-5}	8.69×10^{-3}	1.83×10^{-4}
VL-CEU	3.27×10^{-3}	1.72×10^{-5}	4.13×10^{-3}	3.29×10^{-5}	3.52×10^{-3}	1.95×10^{-5}
VL-CU	3.50×10^{-3}	1.94×10^{-5}	3.28×10^{-3}	1.76×10^{-5}	3.84×10^{-3}	2.33×10^{-5}
Panel C: H = 5						
LSTM	1.10×10^{-2}	1.99×10^{-4}	1.04×10^{-2}	1.88×10^{-4}	1.24×10^{-2}	3.67×10^{-4}
LSTM-CEU	1.09×10^{-2}	1.97×10^{-4}	1.04×10^{-2}	1.80×10^{-4}	1.23×10^{-2}	3.62×10^{-4}
LSTM-CU	1.08×10^{-2}	1.98×10^{-4}	1.02×10^{-2}	1.77×10^{-4}	1.22×10^{-2}	3.62×10^{-4}
CLA	1.11×10^{-2}	2.19×10^{-4}	1.10×10^{-2}	2.04×10^{-4}	1.77×10^{-2}	7.17×10^{-4}
CLA-CEU	1.09×10^{-2}	2.06×10^{-4}	1.04×10^{-2}	1.81×10^{-4}	1.25×10^{-2}	3.48×10^{-4}
CLA-CU	1.10×10^{-2}	2.14×10^{-4}	1.05×10^{-2}	1.85×10^{-4}	1.28×10^{-2}	3.51×10^{-4}
VL	6.25×10^{-3}	6.38×10^{-5}	6.55×10^{-3}	7.45×10^{-4}	8.63×10^{-3}	1.59×10^{-4}
VL-CEU	4.08×10^{-3}	3.48×10^{-5}	3.45×10^{-3}	2.10×10^{-5}	4.52×10^{-3}	3.41×10^{-5}
VL-CU	3.44×10^{-3}	1.90×10^{-5}	3.90×10^{-3}	2.46×10^{-5}	4.59×10^{-3}	3.35×10^{-5}

Note: The underlined numbers indicate that the corresponding model has the lowest loss-function value among all the models.

Table 6
Wilcoxon signed-rank test results.

Models	CSI New-Energy		CNI New-Energy		CN New-Energy	
	MAE	MSE	MAE	MSE	MAE	MSE
LSTM-CEU	+	+	+	+	+	+
LSTM-CU	+	+	+	+	+	+
CLA	+	+	+	+	+	+
CLA-CEU	+	+	+	+	+	+
CLA-CU	+	+	+	+	+	+
VL	+	+	+	+	+	+
VL-CEU	+	+	+	+	+	+
VL-CU	+	+	+	+	+	+

Notes: Wilcoxon signed-rank test results indicating the worse (−), better (+), and equivalent (≈) than the LSTM model in Predicting China New-Energy Index Volatility.

Table 7
DM test results of the model before and after adding the climate risk indicator (LSTM).

Models	CSI New-Energy		CNI New-Energy		CN New-Energy	
	MAE	MSE	MAE	MSE	MAE	MSE
Panel A: LSTM (A) and LSTM-CEU (B)						
1-step	1.171*	2.606^{**}	1.909*	3.528^{***}	1.791*	3.299^{***}
2-step	1.150*	3.872^{***}	2.658^{**}	5.105^{***}	1.753*	3.288^{***}
3-step	1.142*	3.305^{***}	2.493^{**}	4.122^{***}	2.088*	2.016^{**}
Panel B: LSTM (A) and LSTM-CU (B)						
1-step	1.202*	4.440^{***}	3.473^{***}	4.263^{***}	1.596*	2.671^{***}
2-step	2.383^{**}	5.659^{***}	3.104^{***}	4.700^{***}	1.715*	2.541^{**}
3-step	1.787*	4.946^{***}	3.320^{***}	4.234^{***}	1.629*	1.766*

Note: *, **, and *** denote, respectively, *p-value* < 0.1, *p-value* < 0.05, and *p-value* < 0.01.

Table 8
DM test results of the model before and after adding the climate risk indicator (CLA).

Models	CSI New-Energy		CNI New-Energy		CN New-Energy	
	MAE	MSE	MAE	MSE	MAE	MSE
Panel A: CLA (A) and CLA-CEU (B)						
1-step	3.083***	1.504*	3.056***	1.370*	3.684***	3.900***
2-step	3.327***	1.577*	3.125***	1.316*	5.219***	5.905***
3-step	3.081***	1.450*	2.730***	1.161*	4.154***	2.493**
Panel B: CLA (A) and CLA-CU (B)						
1-step	4.052***	2.538**	4.453***	4.135***	3.944***	3.988***
2-step	4.088***	2.915***	4.087***	3.444***	4.945***	4.840***
3-step	3.928***	2.744***	3.722***	2.903***	3.863***	2.452**

Note: *, **, and *** denote, respectively, *p-value* < 0.1, *p-value* < 0.05, and *p-value* < 0.01.

Table 9
DM test results of the model before and after adding the climate risk indicator (VL).

Models	CSI New-Energy		CNI New-Energy		CN New-Energy	
	MAE	MSE	MAE	MSE	MAE	MSE
Panel A: VL (A) and VL-CEU (B)						
1-step	1.672*	2.098**	2.978***	2.803***	3.562***	2.427**
2-step	3.772***	3.828***	3.246***	2.248**	6.343***	3.613***
3-step	2.699***	1.965*	5.812***	4.551***	5.195***	2.958***
Panel B: VL (A) and VL-CU (B)						
1-step	2.105**	2.524**	3.061***	2.887***	3.437***	2.358**
2-step	3.493***	3.435***	4.738***	5.391***	6.569***	3.601***
3-step	3.425***	3.334***	4.485***	4.586***	4.870***	2.915***

Note: *, **, and *** denote, respectively, *p-value* < 0.1, *p-value* < 0.05, and *p-value* < 0.01.

Fig. 3 shows the decomposed subsequence, where each IMF component is sorted from high to low frequency, with Res as the residual term. All subsequences fluctuated around zero, making them easier to forecast. In addition, the VMD results showed that the RV series of the China New-Energy Index contained a significant amount of noise.

The descriptive statistics in Table 4 show that the original series of China's three new-energy indices have small standard deviations after VMD, while the Ljung–Box statistic is significant at the 1 % level, confirming the sequential correlation in these subseries.

4. Empirical results

According to Keskar et al. (2016), we set the learning rate of the LSTM model to 0.001 and the batch size (mini-batch) to 32 to balance low computation and better prediction performance. Egorov et al. (2006) found that the in-sample test was prone to data mining bias, while the out-of-sample prediction method based on a rolling window could avoid such bias, and the latest data could be used to predict all time points out of the sample, thereby ensuring the robustness of the prediction results. Thus, we adopted the rolling time prediction method in this study to test the prediction performance of the aforementioned model. Therefore, referring to the setting of Lin et al. (2022), each subsequence was first divided into training, validation, and prediction sets at a 7:2:1 ratio in the empirical part. The data of the training set were then input into the corresponding LSTM prediction model for training. Finally, we used the data from the prediction set to obtain the results.

4.1. Role of climate risk indicators

We selected the MAE and MSE indicators for comparison to verify the forecasting effect of the climate risk index on the RV of China's new-energy indices. Considering the robustness of the prediction results, we selected different window lengths to represent different prediction periods to enhance the credibility of the results by setting them one step ahead for the short-term, three steps ahead for the medium term, and five steps ahead for the long-term. Table 5 shows the out-of-sample prediction results for models with and without climate risk indicators. The results show that the VL model outperformed the LSTM and CLA models for forecasting without climate risk indicators, and the model performed best for the one-, three-, and five-step-ahead forecasting and all the analyzed RVs of China's new-energy indices. This may have been because the VMD algorithm fully considered the narrow-band nature of the components; therefore, the filtering bands were more concentrated, the obtained IMF components had higher signal-to-noise ratios, and the feature information input into the LSTM model was more adequate.

In addition, when we added the climate risk indicator to the prediction model, the prediction effect of all models improved, and the superiority of the VL model was verified. Under the VL model with CEU indicators, the MAE values of the three new-energy indices

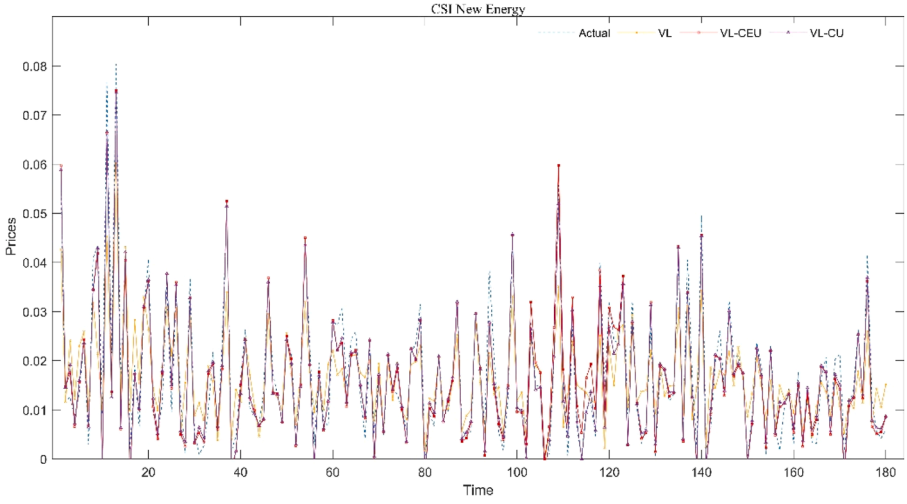

(a) CSI New-Energy Index

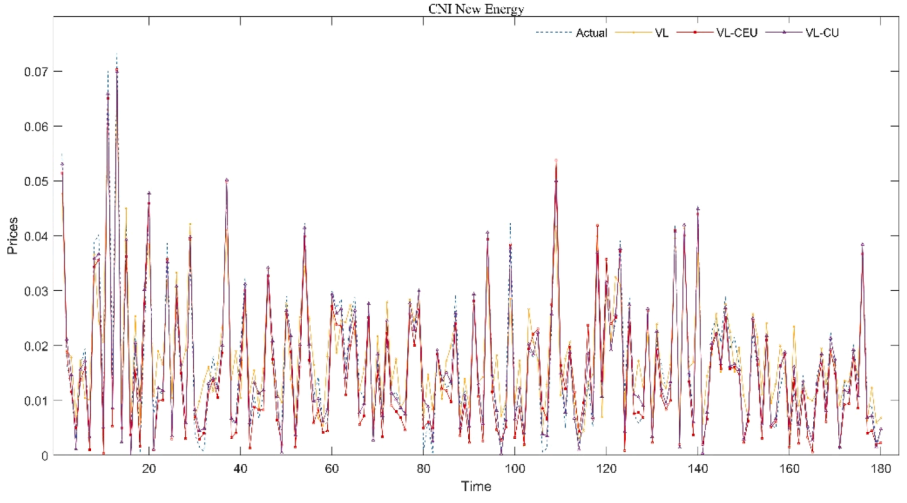

(b) CNI New-Energy Index

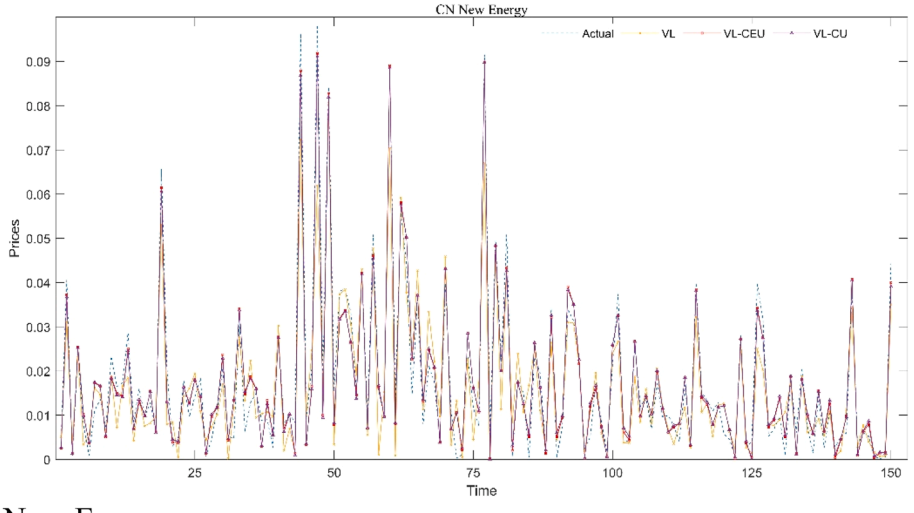

(c) CN New-Energy

(caption on next page)

Fig. 4. Comparison of forecast results.

with one step ahead were reduced by 8.3 %, 16.7 %, and 18.6 %, respectively, and the MSE values for one step ahead were reduced by 19.6 %, 38.2 %, and 32.9 %, respectively. However, under the VL model with CU indicators, the MAE values of the three new-energy indices for one step ahead were reduced by 8.1 %, 17.3 %, and 18.4 %, respectively, and the MSE values for one step ahead were reduced by 20.3 %, 40.0 %, and 32.4 %, respectively. The performances under the three-step-ahead and five-step-ahead scenarios also improved significantly, emphasizing that adding the climate risk indicator can provide new forecasting information about the RV of the new-energy market in China. For the LSTM and CLA models, adding the CEU and CU metrics improved forecasting performance, confirming improvements in the forecasting performance of each model over different periods. While the CU metrics improved the forecasting effect of the CSI New-Energy and CNI New-Energy indices more effectively, the CEU metrics improved the forecasting effect of the CN New-Energy Index.

Because LSTM models are stochastic, we conducted a nonparametric Wilcoxon signed-rank test. Table 6 presents the results of the test, confirming that the LSTM model exhibited statistically lowest MAE and MSE values than the other forecasting models employed in this study, and further substantiating the reliability of our conclusions.

We verified the importance of including climate risk indicators in the forecasting task using the DM test and used the *p-value* to determine whether the original hypothesis with the same level of accuracy could be rejected. Positive DM coefficients indicated that model (B) was superior to model (A).

In this study, we tested the statistical significance of differences among the LSTM, CLA, and VL models with and without climate risk indicators. Tables 7–9 present the results of the DM test and emphasize the statistical significance of the improvement in forecasting performance for the RV of the three Chinese new-energy indices at all lead times for both CEU and CU. Thus, the test confirms that including a measure of climate risk significantly improved the forecasting accuracy of RV in the Chinese new-energy market.

In this study, we visualized the importance of climate risk indicators in forecasting RV in China's new-energy market. Fig. 4 shows that all three of China's new-energy indices improved their fit to the true value after adding the CEU or CU indicators, reiterating the reliability of the findings of this study.

Finally, in this study, we used the MCS test to validate the finding that the addition of climate risk indicators can improve the accuracy of volatility forecasts in the Chinese new-energy market. We set the bootstraps to 1000 and the length of blocks to 12 to generate the *p-value* in the MCS. Furthermore, we set the significance level of the *p-value* to 0.25; that is, only when the model's *p-value* was greater than 0.25 was it retained. The closer the value was to 1, the better the performance of the model. Table 10 lists the results of the MCS tests, showing that regardless of the long, medium, or short-term, the VL model with the climate risk indicator had a maximum value of one for both the MAE and MSE loss indicators, and the *p-values* were maximized at 1. In addition, the VL-CEU and VL-CU models passed the MCS test in most cases. For CSI New-Energy and CNI New-Energy, the prediction of the CU indicator improved more than that of the CEU indicator, while for CN New-Energy Index, the prediction of the CEU indicator improved.

There are several explanations for these results. First, the frequency and severity of extreme weather events have fueled fears of climate catastrophes, thereby increasing the demand for new-energy sources. New-energy sources are relatively independent of climatic factors and carry lower risks than traditional energy sources, thus increasing investor interest in the new-energy market and the pace of China's transition to new-energy sources. Second, policy changes require considerable time. Consequently, investors perceive the risk of climate policy changes gradually rather than suddenly. In this case, the impact of CEUs on the new-energy market may have already been captured by RV, thus failing to provide sufficient additional information for forecasting RV. Finally, the data may have affected the results. As the CN New-Energy Index was selected in 2016, and Chinese investors' concerns regarding the risks posed by climate change have gradually increased since the release of the Paris Agreement on December 12, 2015, the CU index has a slightly lower impact on the CN New-Energy Index than the CEU index does.

4.2. Robustness tests

4.2.1. Adjusting the sample ratio for model training, testing, and prediction

Considering that the data ratio setting in the LSTM model could affect the prediction results, we adjusted the ratio of the training, test, and prediction sets and changed the allocation ratio from 7:2:1–6:2:2. The DM test results in Tables 11–13 indicate that both the CEU and CU metrics improved the prediction effect of the three models on the RV of the three new-energy indices. Table 14 confirms that the CU indicator performed optimally in improving the prediction of RV of CSI New-Energy and CNI New-Energy. These results demonstrate that the conclusions presented in this study remained robust, despite the change in the proportion of data in the LSTM model.

4.2.2. Exclusion of data during the COVID-19 outbreak

To improve the reliability of the empirical findings, we excluded data from the CSI New-Energy and CNI New-Energy indices for the COVID-19 outbreak in China. The results of the DM test in Tables 15–17 and of the MCS test in Table 18 show that the VL model still

Table 10
Out-of-sample results based on the MCS test.

Models	CSI New-Energy				CNI New-Energy				CN New-Energy			
	MAE		MSE		MAE		MSE		MAE		MSE	
	T_R	T_{SQ}	T_R	T_{SQ}	T_R	T_{SQ}	T_R	T_{SQ}	T_R	T_{SQ}	T_R	T_{SQ}
Panel A: H = 1												
LSTM	0.000	0.001	0.001	0.006	0.001	0.000	0.000	0.003	0.000	0.001	0.039	0.014
LSTM-CEU	0.000	0.000	0.009	0.019	0.001	0.000	0.002	0.006	0.000	0.001	0.039	0.015
LSTM-CU	0.000	0.001	0.033	0.024	0.001	0.000	0.025	0.012	0.000	0.001	0.039	0.015
CLA	0.000	0.000	0.001	0.004	0.000	0.000	0.002	0.004	0.001	0.001	0.003	0.006
CLA-CEU	0.000	0.000	0.001	0.006	0.001	0.000	0.000	0.003	0.001	0.001	0.039	0.017
CLA-CU	0.000	0.000	0.001	0.011	0.001	0.000	0.002	0.006	0.001	0.001	0.003	0.006
VL	0.006	0.009	0.043	0.040	0.002	0.000	0.031	0.020	0.001	0.001	0.040	0.031
VL-CEU	0.463	0.463	0.647	0.647	0.714	0.714	0.666	0.666	**1.000**	**1.000**	**1.000**	**1.000**
VL-CU	**1.000**	**1.000**	**1.000**	**1.000**	**1.000**	**1.000**	**1.000**	**1.000**	0.287	0.287	0.778	0.778
Panel B: H = 3												
LSTM	0.000	0.000	0.000	0.000	0.000	0.000	0.000	0.001	0.000	0.000	0.015	0.007
LSTM-CEU	0.000	0.000	0.000	0.000	0.000	0.000	0.000	0.002	0.000	0.000	0.015	0.007
LSTM-CU	0.000	0.000	0.000	0.000	0.000	0.000	0.000	0.002	0.000	0.000	0.015	0.007
CLA	0.000	0.000	0.000	0.000	0.000	0.000	0.000	0.001	0.000	0.000	0.001	0.001
CLA-CEU	0.000	0.000	0.000	0.000	0.000	0.000	0.000	0.002	0.000	0.000	0.015	0.007
CLA-CU	0.000	0.000	0.000	0.000	0.000	0.000	0.000	0.002	0.000	0.000	0.015	0.007
VL	0.007	0.004	0.002	0.001	0.000	0.000	0.000	0.002	0.000	0.000	0.015	0.007
VL-CEU	**1.000**	**1.000**	**1.000**	**1.000**	0.292	0.292	0.270	0.270	**1.000**	**1.000**	**1.000**	**1.000**
VL-CU	0.404	0.404	0.476	0.476	**1.000**	**1.000**	**1.000**	**1.000**	0.037	0.037	0.023	0.023
Panel C: H = 5												
LSTM	0.000	0.000	0.000	0.000	0.000	0.000	0.000	0.000	0.000	0.000	0.015	0.007
LSTM-CEU	0.000	0.000	0.000	0.000	0.000	0.000	0.000	0.000	0.000	0.000	0.015	0.007
LSTM-CU	0.000	0.000	0.000	0.000	0.000	0.000	0.000	0.000	0.000	0.000	0.015	0.007
CLA	0.000	0.000	0.000	0.000	0.000	0.000	0.000	0.000	0.000	0.000	0.001	0.001
CLA-CEU	0.000	0.000	0.000	0.000	0.000	0.000	0.000	0.000	0.000	0.000	0.015	0.007
CLA-CU	0.000	0.000	0.000	0.000	0.000	0.000	0.000	0.000	0.000	0.000	0.015	0.007
VL	0.000	0.000	0.000	0.000	0.000	0.000	0.000	0.000	0.000	0.000	0.015	0.007
VL-CEU	0.466	0.466	0.300	0.300	**1.000**	**1.000**	**1.000**	**1.000**	**1.000**	**1.000**	**1.000**	**1.000**
VL-CU	**1.000**	**1.000**	**1.000**	**1.000**	0.308	0.308	0.554	0.554	0.415	0.415	0.023	0.023

Note: This table shows the out-of-sample prediction accuracies based on the MCS test; bold numbers indicate that the corresponding model had the best prediction performance under the MCS. *P-value* greater than 0.25 are underlined. $H = 1$, 3, and 5 represent one-, three-, and five steps ahead, respectively. T_R and T_{SQ} denote the range and semiquadratic statistics, respectively (Hansen et al., 2011).

Table 11
DM test results of the model at 6:2:2 ratio (LSTM).

Models	CSI New-Energy		CNI New-Energy		CN New-Energy	
	MAE	MSE	MAE	MSE	MAE	MSE
Panel A: LSTM (A) and LSTM-CEU (B)						
1-step	1.254*	2.755***	1.381*	2.394**	3.462***	6.188***
2-step	1.533*	3.394***	1.301*	2.463**	2.547***	4.687***
3-step	1.691*	4.383***	1.161*	2.686***	2.155**	3.799***
Panel B: LSTM (A) and LSTM-CU (B)						
1-step	2.024**	4.622***	3.482***	2.104**	3.187***	5.779***
2-step	2.486**	4.622***	3.364***	2.246**	2.375**	4.189***
3-step	2.889***	5.455***	2.938***	2.344**	1.979*	3.361***

Note: *, **, and *** denote *p-value* < 0.1, *p-value* < 0.05, and *p-value* < 0.01, respectively.

Table 12
DM test results of the model at 6:2:2 ratio (CLA).

Models	CSI New-Energy		CNI New-Energy		CN New-Energy	
	MAE	MSE	MAE	MSE	MAE	MSE
Panel A: CLA and CLA-CEU						
1-step	3.287***	2.111**	2.904***	1.970*	2.471**	1.713*
2-step	2.927***	2.005**	2.477**	1.706*	3.646***	2.632***
3-step	2.517**	1.722*	2.218**	1.464*	3.916***	3.520***
Panel B: CLA and CLA-CU						
1-step	5.690***	4.148***	6.808***	7.087***	1.858*	1.354*
2-step	6.627***	4.886***	7.390***	6.252***	3.339***	2.573***
3-step	6.254***	4.707***	6.565***	5.588***	3.469***	3.439***

Note: *, **, and *** denote *p-value* < 0.1, *p-value* < 0.05, and *p-value* < 0.01, respectively.

Table 13
DM test results of the model at 6:2:2 ratio (VL).

Models	CSI New-Energy		CNI New-Energy		CN New-Energy	
	MAE	MSE	MAE	MSE	MAE	MSE
Panel A: VL (A) and VL-CEU (B)						
1-step	4.405***	4.604***	4.108***	4.374***	5.602***	5.727***
2-step	3.343***	1.896	4.255***	2.236**	7.063***	6.015***
3-step	4.239***	1.857	3.628***	1.679*	6110***	6.292***
Panel B: VL (A) and VL-CU (B)						
1-step	4.976***	4.930***	5.537***	5.416***	5.596***	5.706***
2-step	5.728***	6.532***	6.415***	6.031***	6.409***	5.893***
3-step	5.257***	6.368***	6.113***	4.819***	5.629***	6.419***

Note: *, **, and *** denote *p-value* < 0.1, *p-value* < 0.05, and *p-value* < 0.01, respectively.

includes an optimally performing climate risk index, confirming the reliability of the findings of this study.

5. Conclusion

Climate risk has attracted widespread attention from the global financial community, particularly academics, central banks, and investors. The new-energy market, as a crucial area in which climate change has to be addressed, is driven by policy and technological innovation and becoming an important investment area in the financial market. In this study, we used a deep-learning model to measure climate risk by selecting the following two indicators: the Chinese CEU and the CU indices to explore how climate risk can predict the volatility of the Chinese new-energy market.

First, the empirical results show that both climate factors, CEU and CU, can effectively improve the prediction accuracy of the RV in the Chinese new-energy market. The CU indicator was more effective in improving the prediction of the CSI New-Energy and CNI New-Energy indices, while the CEU indicator was better in improving the prediction of the CN New-Energy Index, possibly because the frequency and severity of extreme weather events triggered concerns regarding climate disasters, thus increasing the demand for new-energy. New-energy sources are independent of climatic factors and carry lower risks than traditional energy sources; therefore, investors are paying more attention to the new-energy market, boosting the pace of China's transition to new-energy sources. Second, policy changes require considerable time. Therefore, investors perceive the risk of climate policy changes gradually rather than

Table 14
MCS test results of the model at 6:2:2 ratio.

Models	CSI New-Energy				CNI New-Energy				CN New-Energy			
	MAE		MSE		MAE		MSE		MAE		MSE	
	T_R	T_{SQ}	T_R	T_{SQ}	T_R	T_{SQ}	T_R	T_{SQ}	T_R	T_{SQ}	T_R	T_{SQ}
Panel A: H = 1												
LSTM	0.000	0.000	0.001	0.001	0.000	0.000	0.000	0.000	0.000	0.000	0.001	0.001
LSTM-CEU	0.000	0.000	0.001	0.001	0.000	0.000	0.000	0.000	0.000	0.000	0.001	0.001
LSTM-CU	0.000	0.000	0.002	0.001	0.000	0.000	0.000	0.000	0.000	0.000	0.001	0.001
CLA	0.000	0.000	0.000	0.000	0.000	0.000	0.000	0.000	0.000	0.000	0.001	0.001
CLA-CEU	0.000	0.000	0.001	0.001	0.000	0.000	0.000	0.000	0.000	0.000	0.001	0.001
CLA-CU	0.000	0.000	0.000	0.000	0.000	0.000	0.000	0.000	0.000	0.000	0.001	0.001
VL	0.000	0.000	0.002	0.001	0.000	0.000	0.000	0.000	0.009	0.003	0.009	0.006
VL-CEU	**1.000**	**1.000**	**1.000**	**1.000**	0.626	0.626	0.614	0.614	0.088	0.088	0.082	0.082
VL-CU	0.449	0.449	0.251	0.251	**1.000**	**1.000**	**1.000**	**1.000**	**1.000**	**1.000**	**1.000**	**1.000**
Panel B: H = 3												
LSTM	0.000	0.000	0.000	0.000	0.000	0.000	0.000	0.000	0.000	0.000	0.000	0.000
LSTM-CEU	0.000	0.000	0.000	0.000	0.000	0.000	0.000	0.000	0.000	0.000	0.000	0.000
LSTM-CU	0.000	0.000	0.000	0.000	0.000	0.000	0.000	0.000	0.000	0.000	0.000	0.000
CLA	0.000	0.000	0.000	0.000	0.000	0.000	0.000	0.000	0.000	0.000	0.000	0.000
CLA-CEU	0.000	0.000	0.000	0.000	0.000	0.000	0.000	0.000	0.000	0.000	0.000	0.000
CLA-CU	0.000	0.000	0.000	0.000	0.000	0.000	0.000	0.000	0.000	0.000	0.000	0.000
VL	0.000	0.000	0.000	0.000	0.000	0.000	0.000	0.000	0.000	0.000	0.000	0.000
VL-CEU	0.036	0.036	0.074	0.074	**1.000**	**1.000**	**1.000**	**1.000**	**1.000**	**1.000**	**1.000**	**1.000**
VL-CU	**1.000**	**1.000**	**1.000**	**1.000**	0.758	0.758	0.515	0.515	0.001	0.001	0.000	0.000
Panel C: H = 5												
LSTM	0.000	0.000	0.000	0.000	0.000	0.000	0.000	0.000	0.000	0.000	0.000	0.000
LSTM-CEU	0.000	0.000	0.000	0.000	0.000	0.000	0.000	0.000	0.000	0.000	0.000	0.000
LSTM-CU	0.000	0.000	0.000	0.000	0.000	0.000	0.000	0.000	0.000	0.000	0.000	0.000
CLA	0.000	0.000	0.000	0.000	0.000	0.000	0.000	0.000	0.000	0.000	0.000	0.000
CLA-CEU	0.000	0.000	0.000	0.000	0.000	0.000	0.000	0.000	0.000	0.000	0.000	0.000
CLA-CU	0.000	0.000	0.000	0.000	0.000	0.000	0.000	0.000	0.000	0.000	0.000	0.000
VL	0.000	0.000	0.000	0.000	0.000	0.000	0.000	0.000	0.000	0.000	0.000	0.000
VL-CEU	0.243	0.243	0.141	0.141	0.896	0.896	0.320	0.320	0.002	0.002	**1.000**	**1.000**
VL-CU	**1.000**	**1.000**	**1.000**	**1.000**	**1.000**	**1.000**	**1.000**	**1.000**	**1.000**	**1.000**	0.001	0.001

Note: This table shows the out-of-sample prediction accuracies based on the MCS test; bold numbers indicate that the corresponding model had the best prediction performance under the MCS. *p-values* greater than 0.25 are underlined. $H = 1$, 3, and 5 represent one-, three-, and five steps ahead, respectively. T_R and T_{SQ} denote the range and semiquadratic statistics, respectively (Hansen et al., 2011).

Table 15
DM test results of the model after excluding data during the pandemic period (LSTM).

Models	CSI New-Energy		CNI New-Energy	
	MAE	MSE	MAE	MSE
Panel A: LSTM (A) and LSTM-CEU (B)				
1-step	2.481**	2.346**	4.319***	2.994***
2-step	1.876*	1.843*	4.616***	3.749***
3-step	1.699*	1.708*	4.950***	8.542***
Panel B: LSTM (A) and LSTM-CU (B)				
1-step	3.345***	3.348***	4.678***	3.587***
2-step	2.865***	3.181***	5.179***	4.523***
3-step	2.974***	3.799***	6.176***	8.785***

Note: *, **, and *** denote *p-value* < 0.1, *p-value* < 0.05, and *p-value* < 0.01, respectively.

Table 16
DM test results of the model after excluding data during the pandemic period (CLA).

Models	CSI New-Energy		CNI New-Energy	
	MAE	MSE	MAE	MSE
Panel A: CLA (A) and CLA-CEU (B)				
1-step	2.481**	2.346**	5.016***	3.929***
2-step	1.876*	1.843*	4.589***	4.589***
3-step	1.699*	1.708*	4.601***	7.083***
Panel B: CLA (A) and CLA-CU (B)				
1-step	3.345***	3.348***	3.392***	2.723***
2-step	2.865***	3.181***	3.096***	3.062***
3-step	2.974***	3.799***	3.428***	5.616***

Note: *, **, and *** denote *p-value* < 0.1, *p-value* < 0.05, and *p-value* < 0.01, respectively.

Table 17
DM test results of the model after excluding data during the pandemic period (VL).

Models	CSI New-Energy		CNI New-Energy	
	MAE	MSE	MAE	MSE
Panel A: VL and VL-CEU				
1-step	6.030***	4.514***	8.194***	7.441***
2-step	5.630***	5.320***	7.192***	8.970***
3-step	4.567***	4.008***	7.425***	7.259***
Panel B: VL and VL-CU				
1-step	6.075***	5.083***	8.133***	8.042***
2-step	5.202***	5.215***	7.134***	8.130***
3-step	4.273***	3.928***	6.483***	6.623***

Note: *, **, and *** denote, *p-value* < 0.1, *p-value* < 0.05, and *p-value* < 0.01, respectively.

suddenly. In such a case, the impact of the CEU index on the new-energy market may have already been captured by RV, thus failing to provide sufficient additional information to forecast RV. Finally, the data may have affected the results. As the CN New-Energy Index was selected in 2016 and Chinese investors' concerns regarding the risks posed by climate change have gradually increased since the release of the Paris Agreement on December 12, 2015, the CU index has a slightly lower impact on the CN New-Energy Index than that of the CEU index.

This study deepens the general understanding of the relationship between climate risk and China's new-energy market from the perspective of integrating climatic factors into volatility forecasting models, confirms the necessity of incorporating climatic factors into forecasting models, and enriches the research on climate risk and volatility forecasting in the Chinese new-energy market. Based on the empirical evidence obtained from this study, market participants must pay close attention to weather disaster warnings and improve their investment strategies accordingly. Furthermore, to mitigate the adverse effects of climate change on the market, regulators (such as government and market regulators) must be mindful of the challenges posed by the risk of climate catastrophes and issue timely alerts to market participants.

Despite the improved predictive accuracy achieved by incorporating climatic risk factors and deep-learning models to forecast the volatility of the Chinese new-energy market, several limitations remain. First, deep-learning models are highly sensitive to hyperparameter selection, and different hyperparameter configurations, such as learning rate, batch size, number of layers, and activation functions, can significantly affect the results. Hence, future studies should focus on optimizing the hyperparameter tuning process to

Table 18
MCS test results of the model after excluding data during the pandemic period.

Models	CSI New-Energy				CNI New-Energy			
	MAE		MSE		MAE		MSE	
	T_R	T_{SQ}	T_R	T_{SQ}	T_R	T_{SQ}	T_R	T_{SQ}
Panel A: H = 1								
LSTM	0.000	0.000	0.000	0.000	0.000	0.000	0.000	0.000
LSTM-CEU	0.000	0.000	0.000	0.000	0.000	0.000	0.000	0.000
LSTM-CU	0.000	0.000	0.000	0.000	0.000	0.000	0.000	0.000
CLA	0.000	0.000	0.000	0.000	0.000	0.000	0.000	0.000
CLA-CEU	0.000	0.000	0.000	0.000	0.000	0.000	0.000	0.000
CLA-CU	0.000	0.000	0.000	0.000	0.000	0.000	0.000	0.000
VL	0.000	0.000	0.000	0.000	0.000	0.000	0.000	0.000
VL-CEU	0.443	0.443	0.016	0.016	0.001	0.001	0.000	0.000
VL-CU	**1.000**	**1.000**	**1.000**	**1.000**	**1.000**	**1.000**	**1.000**	**1.000**
Panel B: H = 3								
LSTM	0.000	0.000	0.000	0.000	0.000	0.000	0.000	0.000
LSTM-CEU	0.000	0.000	0.000	0.000	0.000	0.000	0.000	0.000
LSTM-CU	0.000	0.000	0.000	0.000	0.000	0.000	0.000	0.000
CLA	0.000	0.000	0.000	0.000	0.000	0.000	0.000	0.000
CLA-CEU	0.000	0.000	0.000	0.000	0.000	0.000	0.000	0.000
CLA-CU	0.000	0.000	0.000	0.000	0.000	0.000	0.000	0.000
VL	0.000	0.000	0.000	0.000	0.000	0.000	0.000	0.000
VL-CEU	0.000	0.000	0.000	0.000	0.000	0.000	0.000	0.000
VL-CU	**1.000**	**1.000**	**1.000**	**1.000**	**1.000**	**1.000**	**1.000**	**1.000**
Panel C: H = 5								
LSTM	0.000	0.000	0.000	0.000	0.000	0.000	0.000	0.000
LSTM-CEU	0.000	0.000	0.000	0.000	0.000	0.000	0.000	0.000
LSTM-CU	0.000	0.000	0.000	0.000	0.000	0.000	0.000	0.000
CLA	0.000	0.000	0.000	0.000	0.000	0.000	0.000	0.000
CLA-CEU	0.000	0.000	0.000	0.000	0.000	0.000	0.000	0.000
CLA-CU	0.000	0.000	0.000	0.000	0.000	0.000	0.000	0.000
VL	0.000	0.000	0.000	0.000	0.000	0.000	0.000	0.000
VL-CEU	0.710	0.710	0.000	0.000	0.000	0.000	0.001	0.001
VL-CU	**1.000**	**1.000**	**1.000**	**1.000**	**1.000**	**1.000**	**1.000**	**1.000**

Note: This table shows the out-of-sample prediction accuracies based on the MCS test; bold numbers indicate that the corresponding model had the best prediction performance under the MCS. *p-values* greater than 0.25 are underlined. $H = 1$, 3, and 5 represent one, three, and five steps ahead, respectively. T_R and T_{SQ} denote the range and semiquadratic statistics, respectively (Hansen et al., 2011).

further enhance model performance. Second, this study was solely based on data from the Chinese new-energy market, and the findings may not be directly applicable to other countries or markets, raising questions about the generalizability of the results. Finally, although we employed the CEU and CU indicators in this study to quantify climate risk, these proxies may not capture the full spectrum of climate risk factors. Thus, future research should incorporate additional climate risk dimensions, such as the integration of specific indicators related to both transition and physical climate risks, and explore more comprehensive measures, including policy-induced risks, extreme weather events, and long-term environmental shifts, to improve the robustness of volatility forecasts.

Funding sources

Funding: This work was supported by the Zhejiang Province Philosophy and Social Science Planning Project [24NDJC222YBM]; and the National Social Science Fund of China [22BJY256].

CRediT authorship contribution statement

Li Jianfeng: Writing – review & editing, Formal analysis. **Wei Xiaokun:** Writing – review & editing. **Jiang Wei:** Writing – review & editing, Writing – original draft, Methodology. **Tang Wanqing:** Writing – review & editing, Writing – original draft, Methodology, Data curation.

Declaration of Competing Interest

The authors declare that they have no known competing financial interests or personal relationships that could have appeared to influence the work reported in this paper.

Data availability

Data will be made available on request.

References

Abdoos, A.A., 2016. A new intelligent method based on combination of VMD and ELM for short term wind power forecasting. Neurocomputing 203, 111–120.
Andersen, T.G., Bollerslev, T., 1998. Answering the skeptics: yes, standard volatility models do provide accurate forecasts. Int. Econ. Rev. 39, 885.
Andersen, T.G., Bollerslev, T., Meddahi, N., 2005. Correcting the errors: volatility forecast evaluation using high-frequency data and realized volatilities. Econometrica 73 (1), 279–296.
Bartram, S.M., Hou, K., Kim, S., 2022. Real effects of climate policy: financial constraints and spillovers. J. Financ. Econ. 143, 668.
Berkman, H., Jona, J., Soderstrom, N., 2024. Firm-specific climate risk and market valuation. Account., Organ. Soc. 112, 101547.
Bonato, M., Cepni, O., Gupta, R., Pierdzioch, C., 2023. Climate risks and realized volatility of major commodity currency exchange rates. J. Financ. Mark. 62, 100760.
Diebold, F.X., Mariano, R.S., 2002. Comparing predictive accuracy. J. Bus. Econ. Stat. 20, 134.
Dragomiretskiy, K., Zosso, D., 2014. Variational mode decomposition. IEEE Trans. Signal Process. 62, 531.
Egorov, A.V., Hong, Y., Li, H., 2006. Validating forecasts of the joint probability density of bond yields: Can affine models beat random walk? J. Econ. 135, 255.
Fan, G.F., Zhang, R.T., Cao, C.C., Peng, L.L., Yeh, Y.H., Hong, W.C., 2024. The volatility mechanism and intelligent fusion forecast of new energy stock prices. Financ. Innov. 10, 84.
Gamboa, J.C., 2017. Deep Learn. Time-Ser. Anal. arXiv, abs/1701.01887.
Gu, Q., Li, S., Tian, S., Wang, Y., 2024. Impact of climate risk on energy market risk spillover: Evidence from dynamic heterogeneous network analysis. Energy Econ. 137, 107775.
Guo, K., Liu, F., Sun, X., Zhang, D., Ji, Q., 2023. Predicting natural gas futures' volatility using climate risks. Financ. Res. Lett. 55, 103915.
Guo, X., Huang, Y., Liang, C., Umar, M., 2022. Forecasting volatility of EUA futures: New evidence. Energy Econ. 110, 106021.
Gupta, R., Pierdzioch, C., 2022. Climate risks and forecastability of the realized volatility of gold and other metal prices. Resour. Policy 77, 102681.
Hansen, P.R., Lunde, A., Nason, J.M., 2011. The model confidence set. Econometrica 79, 453.
He, F., Zhou, J., Feng, Z., Liu, G., Yang, Y., 2019. A hybrid short-term load forecasting model based on variational mode decomposition and long short-term memory networks considering relevant factors with Bayesian optimization algorithm. Appl. Energy 237, 103.
Herrera, G.P., Constantino, M., Su, J.J., Naranpanawa, A., 2022. Renewable energy stocks forecast using Twitter investor sentiment and deep learning. Energy Econ. 114, 106285.
Hertwich, E.G., Gibon, T., Bouman, E.A., Arvesen, A., Suh, S., Heath, G.A., Bergesen, J.D., Ramirez, A., Vega, M.I., Shi, L., 2015. Integrated life-cycle assessment of electricity-supply scenarios confirms global environmental benefit of low-carbon technologies. Proc. Natl. Acad. Sci. USA 112, 6277.
Huang, N., Wu, Y., Cai, G., Zhu, H., Yu, C., Jiang, L., Zhang, Y., Zhang, J., Xing, E., 2019. Short-term wind speed forecast with low loss of information based on feature generation of OSVD. IEEE Access 7, 81027.
Huang, Y., Xu, W., Huang, D., Zhao, C., 2023. Chinese crude oil futures volatility and sustainability: An uncertainty indices perspective. Resour. Policy 80, 103227.
Isah, K., Odebode, A., Ogunjemilua, O., 2023. Does climate risk amplify oil market volatility? Energy Res. Lett. 4.
Jiang, W., Tang, W., Liu, X., 2023. Forecasting realized volatility of Chinese crude oil futures with a new secondary decomposition ensemble learning approach. Financ. Res. Lett. 57, 104254.
Jin, J., Han, L., Wu, L., Zeng, H., 2020. The hedging effect of green bonds on carbon market risk. Int. Rev. Financ. Anal. 71, 101509.
Karmakar, S., Gupta, R., Cepni, O., Rognone, L., 2023. Climate risks and predictability of the trading volume of gold: Evidence from an INGARCH model. Resour. Policy 82, 103438.
Keskar, N.S., Mudigere, D., Nocedal, J., Smelyanskiy, M., & Tang, P.T. 2016. On large-batch training for deep learning: Generalization gap and sharp minima. arXiv, abs/1609.04836.
Kristjanpoller, W., 2024. A hybrid econometrics and machine learning based modeling of realized volatility of natural gas. Financ. Innov. 10, 45.
Lahmiri, S., 2017. Comparing variational and empirical mode decomposition in forecasting day-ahead energy prices. IEEE Syst. J. 11, 1907–1910.
Lee, K., Cho, J., 2023. Measuring Chinese climate uncertainty. Int. Rev. Econ. Financ. 88, 891.
Li, C., Zhang, X., Qaosar, M., Ahmed, S., Alam, K.M.R., & Morimoto, Y. 2019, August. Multi-factor based stock price prediction using hybrid neural networks with attention mechanism. in IEEE international conference on dependable, autonomic and secure computing, international conference on pervasive intelligence and computing, international conference on cloud and big data computing, international conference on cyber science and technology congress (dasc/picom/cbdcom/cyberscitech) (pp. 961-966). IEEE.
Liang, C., Umar, M., Ma, F., Huynh, T.L.D., 2022. Climate policy uncertainty and world renewable energy index volatility forecasting. Technol. Forecast. Soc. Change 182, 121810.
Lin, Y., Lin, Z., Liao, Y., Li, Y., Xu, J., Yan, Y., 2022. Forecasting the realized volatility of stock price index: a hybrid model integrating CEEMDAN and LSTM. Expert Syst. Appl. 206, 117736.
Liu, Y., 2019. Novel volatility forecasting using deep learning-long short term memory recurrent neural networks. Expert Syst. Appl. 132, 99.
Liu, Y., Yang, C., Huang, K., Gui, W., 2020. Non-ferrous metals price forecasting based on variational mode decomposition and LSTM network. Knowl. -Based Syst. 188, 105006.
Lv, W., Li, B., 2023. Climate policy uncertainty and stock market volatility: evidence from different sectors. Financ. Res. Lett. 51, 103506.
Rao, A., Lucey, B., Kumar, S., 2023. Climate risk and carbon emissions: Examining their impact on key energy markets through asymmetric spillovers. Energy Econ. 126, 106970.
Sadorsky, P., 2022. Using machine learning to predict clean energy stock prices: how important are market volatility and economic policy uncertainty? J. Clim. Financ. 1, 100002.
Salisu, A.A., Olaniran, A., Lasisi, L., 2023. Climate risk and gold. Resour. Policy 82, 103494.
Tian, H., Long, S., Li, Z., 2022. Asymmetric effects of climate policy uncertainty, infectious diseases-related uncertainty, crude oil volatility, and geopolitical risks on green bond prices. Financ. Res. Lett. 48, 103008.
Wang, J., Li, L., 2023. Climate risk and Chinese stock volatility forecasting: evidence from ESG index. Financ. Res. Lett. 55, 103898.
Xia, Y., Ren, H., Li, Y., Xia, J., He, L., Liu, N., 2022. Forecasting green bond volatility via novel heterogeneous ensemble approaches. Expert Syst. Appl. 204, 117580.
Xu, X., Zhang, Y., 2023. China mainland new energy index price forecasting with the neural network. Energy Nexus 10, 100210.